Journal of Hazardous Materials 166 (2009) 830–835

Contents lists available at ScienceDirect

Journal of Hazardous Materials

journal homepage: www.elsevier.com/locate/jhazmat

Removal of basic dye using raw and acid activated bentonite samples

E. Eren [a,*], B. Afsin [b]

[a] Ahi Evran University, Faculty of Arts and Science, Department of Chemistry, 40100 Kırsehir, Turkey
[b] Ondokuz Mayis University, Faculty of Arts and Science, Department of Chemistry, 55139 Kurupelit/Samsun, Turkey

ARTICLE INFO

Article history:
Received 8 December 2006
Received in revised form 27 October 2008
Accepted 26 November 2008
Available online 14 December 2008

Keywords:
Dye adsorption
Activation thermodynamic
Kinetic
Acid activation
X-ray diffraction

ABSTRACT

The adsorption behavior of crystal violet (CV^+) from aqueous solution onto raw (RB) and acid activated (AAB) bentonite samples was investigated as a function of parameters such as initial CV^+ concentration, contact time and temperature. The Langmuir and Freundlich adsorption models were applied to describe the equilibrium isotherms. The adsorption rate was fast and more than half of the adsorbed-CV^+ was removed in the first 55 min for RB and 25 min for 0.2-AAB at the room temperature (C_0 = 1.2 mmol/g). The pseudo-first order, and pseudo-second order kinetic models were used to describe the kinetic data and rate constants were evaluated. The results best fit the pseudo-second order kinetic model with the rate constant, k_2, in the range of 13.52×10^{-2} to 5.53×10^{-2} g/mmol and 52.70×10^{-2} to 6.69×10^{-2} mmol/g min for RB and 0.2-AAB sample, respectively (C_0 = 0.1–1.2 mmol/g).

© 2008 Elsevier B.V. All rights reserved.

1. Introduction

Basic dyes can be applied to wool, silk and leather [1]. This group dyes can cause allergic dermatitis, skin irritation, cancer, and mutations. There are several methods for dye removals, such as adsorption, oxidation–ozonation, coagulation, coagulation–flocculation and biological methods. Adsorption process provides an attractive alternative treatment to other removal techniques because it is more economical and readily available. Bentonite is widely applied in many fields of adsorption technology including the removal of metals [2,3], phenols [4,5], organic molecules [6,7], polymers [8,9], pesticides [10], radionuclides [11], and dyes [12,13].

Bentonite from Unye, Turkey, was used for this study due to its local abundance and availability for use in Turkish waste water treatment facilities. Although it is possible to increase the surface area and physicochemical activity of bentonite by means of acid activation, the relationship between adsorption kinetics and the structural change of bentonite after acidification using mineral acid is not clear. Therefore, it is very important to study the adsorption of a large organic cations on acid activated bentonite. The aim of this study was to test the adsorption behavior of large organic cation from aqueous solution on acid activated bentonite. The data thus obtained may be helpful to environmental engineers for designing and establishing a continuous treatment plant for water and wastewaters. In order to elucidate the role of the bentonite surface in the CV^+ adsorption process, the effects of initial CV^+ concentration, contact time and temperature were investigated.

2. Experimental

2.1. Materials

2.1.1. Preparation of raw bentonite (RB)

The preparation of RB is already discussed in previous work [13]. Whitness was found to be 85%. RB was composed of 62.70% SiO_2, 20.10% Al_2O_3, 2.16% Fe_2O_3, 2.29%CaO, 3.64% MgO, 0.27%, Na_2O, 2.53% K_2O, 0.21% TiO_2, P_2O_5% 0.02. The ignition loss of the RB at 1273 K was also found to be 7.4%. The cation exchange capacity (CEC), determined with triethanolamine-buffered $BaCl_2$ solution (c = 0.1 M) followed by a reexchange with aqueous $MgCl_2$ solution (c = 0.1 M), is of 0.65 mmol/g [14].

2.1.2. Preparation of acid activated bentonite (AAB)

Twenty grams of RB were activated with various volumes (20, 51, 102 and 204 ml) of 2.0 M H_2SO_4 at 80 °C for 2 h. The acid activated samples were washed thoroughly with deionized water untill pH 5.0. The ratio of RB to H_2SO_4 was changed between 0.2 and 2.0 by mass. Acid activated samples were named as 0.2-AAB (H_2SO_4/RB (w/w) = 0.2), 0.5-AAB (H_2SO_4/RB (w/w) = 0.5), 1.0-AAB (H_2SO_4/RB (w/w) = 1.0) and 2.0-AAB (H_2SO_4/RB (w/w) = 2.0). The clay was then separated from the acid solution, using a centrifugal separator. The separated clay was then resuspended in deionized water and re-separated by centrifugation three times to remove ions and other

* Corresponding author. Tel.: +90 386 211 45 00; fax: +90 386 211 45 25.
E-mail address: eeren@ahievran.edu.tr (E. Eren).

0304-3894/$ – see front matter © 2008 Elsevier B.V. All rights reserved.
doi:10.1016/j.jhazmat.2008.11.132

Nomenclature

AAB	acid activated bentonite
RB	raw bentonite
CV^+	crystal violet
C_e	equilibrium concentration of the adsorbate in the solution (mmol/L)
D_p	average pore diameter
IS	Ionic strength
k_1	first-order rate constant of adsorption (1/h)
k_2	second-order rate constant of adsorption (g/mmol min)
K_L	constant that represents the energy or net enthalpy of adsorption (L/g)
K_F	Freundlich constant indicative of the adsorption capacity of the adsorbent (mmol/g)
m	mass of adsorbent (g/L)
n	experimental constant indicative of the adsorption intensity of the adsorbent
q_e	amount of adsorbate removed from aqueous solution at equilibrium (mmol/g)
q_t	amount of adsorbate sorbed on the sorbent surface at any time t (mmol/g)
q_m	mass of adsorbed solute completely required to saturate a unit mass of adsorbent (mmol/g)
S_{BET}	The BET surface area
S_{ext}	external surface area (including only mesopores)
S_{mic}	micropores surface area
t	reaction time (min)
V_t	total pore volume

residues from the acidification process. The resulting products were finally dried at 105 °C for 24 h, and stored in the desiccator prior to the physical and chemical characterizations. Equilibrium and kinetic studies on the removal of CV^+ were studied by using 0.2-AAB (acid/clay = 0.2).

2.2. Dye adsorption measurement

Adsorption of CV^+ (analytical grade, chloride salt, obtained from Reidel-de Haen) was carried out by a batch technique to obtain equilibrium data. The experiments of adsorption equilibrium and kinetics were carried out as similarly described before [15]. The amount of CV^+ adsorbed (mmol/g), (q_e), onto bentonite was calculated from the mass balance equation as follows:

$$q_e = (C_0 - C_e)\frac{V}{W} \quad (1)$$

where C_0 and C_e are the initial and equilibrium liquid-phase concentrations of dye solution (mol/L), respectively; V the volume of dye solution (mL), and W the mass of bentonite sample used (g).

2.3. Characterization methods

The mineralogical compositions of the RB and 0.2-AAB samples were obtained by powder X-ray diffraction (XRD). XRD measurements were taken with a Rigaku 2000 automated diffractometer using Ni filtered Cu Kα radiation. A Tri Star 3000 (Micromeritics, USA) surface analyzer was also used to measure the nitrogen adsorption isotherm at 77 K in the range of relative pressure 10^{-6} to 1. Before measurement, the sample was degassed at 300 °C for 2 h. The surface areas were calculated by the BET (Brunauer–Emmett–Teller) method. The total pore volume value is 0.07 cm^3/g, the micropores contribute to 11.42% of total pore volume. The average pore diameter is 8.11 nm (Table 1).

Table 1
Porous structure parameters of the RB sample.

Sample	RB
S_{BET} (m^2/g)	36.17
S_{ext}[a] (m^2/g)	19.86
S_{mic} (m^2/g)	16.30
V_t (cm^3/g)	0.07
V_{mic} (cm^3/g)	0.008
V_{meso} (cm^3/g)	0.067
D_p[b] (nm)	8.11

[a] $S_{ext} = S_{meso}$.
[b] 4 V/A by BET.

3. Results and discussion

3.1. Chemical analysis

The bentonite obtained after acid treatment showed a progressive decrease in A1, Mg and Fe (octahedral cations) and an enrichment in SiO_2 coming from the tetrahedral layer of bentonite (Table 2). The enrichment in SiO_2 is a relative increase due to the remobilization of the octahedral cations. The octahedral cations pass into the solution while silica, owing to its insolubility in acid solution, remains in the 0.2-AAB. When RB was activated with acid, 9.45% of the $A1_2O_3$, 23.15% of the Fe_2O_3 and 13.74% of the MgO were removed from the RB. The relative Ti^{4+} content of the activated clay increases greatly by the acid activation. It has been discussed that the Ti^{4+} cations located either octahedral sites or tetrahedral sites [16].

3.2. XRD analysis

The XRD patterns of RB and 0.2-AAB samples are presented in Fig. 1. For the XRD pattern of RB, one reflection was observed in the region $2° < 2\theta < 8°$ (Fig. 1a). This corresponds to the 5.76 (2θ) value from which the interlamellar distance was found to be 15.33 Å. The d_{001} value of 0.2-AAB was found by the shoulder appearing at 5.20° (2θ) in the XRD pattern of the 0.2-AAB (Fig. 1b). The position of d_{001} peak of 0.2-AAB sample shifted from 15.33 to 16.98 Å (Fig. 1b) which was accompained by a intensity decrease from 100 to 68%. The XRD results also show that acid activation has caused structural changes in the treated bentonite. Activation has affected mainly the 001 reflection; the intensity of the 001, 003 and 060 reflections has been reduced, while the intensities of the 020 and 006 reflections has been increased significantly by the acid activation process. The acid activated sample displays an increase of the background in the interval between 20 and 30° due to the deposition of amorphous silica caused after the attack on the octahedral layer and the exposure of the tetrahedral layer. Acid activation of the RB yielded d_{101} reflection at 3.96 Å (2θ = 22.40), which is absent in the RB. Appearance of new reflection indicate the formation of expansible phases and

Table 2
Chemical composition of the bentonite samples.

Sample	SiO_2 (%)	Al_2O_3 (%)	Fe_2O_3 (%)	CaO (%)	MgO (%)	Na_2O (%)	K_2O (%)	TiO_2 (%)	P_2O_5 (%)	LOI (%)
RB	62.70	20.10	2.16	2.29	3.64	0.27	2.53	0.21	0.02	6.10
0.2-AAB	68.12	18.20	1.66	1.69	3.14	0.15	1.78	0.24	0.002	5.02

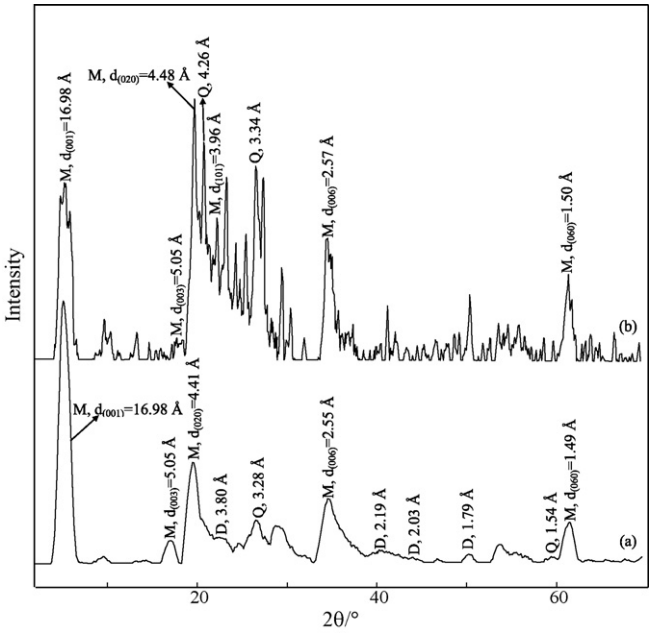

Fig. 1. The X-ray diffraction patterns of the RB (A) and AAB (B) samples (M: montmorillonite, Q: quartz, D: dolomite).

interlamellar expansion [17]. The XRD pattern of the 0.2-AAB shows the partial destruction of the crystal structure compared to the parent clay. Such distortion of clay minerals following acid activation gives rise to an increase in the intensities of the low angle diffraction peaks [17]. Therefore, the XRD pattern of 0.2-AAB shows poor crystallinity, with broadened and more intense peaks compared to the parent clay mineral.

The adsorption of CV^+ on the RB led to significant increase in the basal spacing of the host material, from 15.33 to 21.22 Å, and new shoulders appeared (Fig. 2a). The basal spacing of the CV^+ adsorbed RB is consistent with a bilayer to pseudo trilayer arrangement of adsorbed CV^+ [18–20]. The value of 18.93 Å for 0.2-AAB is consistent with a bilayer arrangement of adsorbed CV^+ [20].

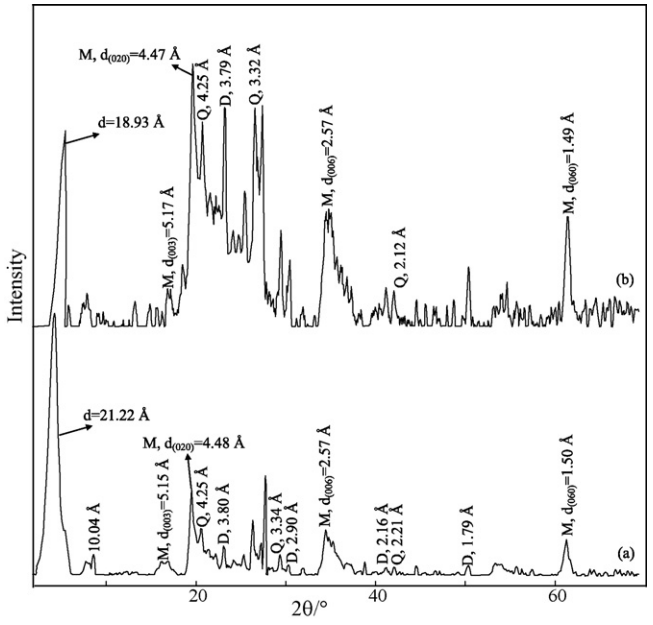

Fig. 2. The X-ray diffraction patterns of the dye-loaded RB (A) and AAB (B) samples (M: montmorillonite, Q: quartz, D: dolomite).

3.3. Langmuir and Freundlich equilibrium isotherm models

The Langmuir and Freundlich isotherm models were applied to the experimental data. The data conform the linear form of Langmuir model (Eq. (2)) [21] expressed below:

$$\frac{C_e}{q_e} = \frac{C_e}{q_m} + \frac{1}{K_L q_m} \quad (2)$$

where C_e is equilibrium concentration of CV^+ (mmol/L) and q_e is the amount of the CV^+ adsorbed (mmol) by per unit of bentonite (g). Linear plots of C_e/q_e vs. C_e (not shown) were employed to determine the value of q_m (mmol/g) and K_L (L/mmol). The Langmuir monolayer adsorption capacities of RB and 0.2-AAB were estimated as 0.51 and 0.23 mmol/g, respectively (Table 3). The lower K_L value for the RB (0.95) compared to that for 0.2-AAB (1.60) indicate that the surface modification process influences the adsorption equilibrium. The high-energy sites with high equilibrium constant (K_L for the 0.2-AAB) had a significantly lower affinity than that for low-energy sites with low equilibrium constant (K_L for the RB). The high-energy sites on which CV^+ was tightly held had a low adsorption maximum (q_m = 0.23 mmol/g), accounting for ≈43% of total CV^+ adsorption on RB. The low energy sites on which dye were loosely held had a high adsorption maximum (q_m = 0.51 mmol/g).

The CV^+ adsorption capacity of SWy-1 was determined to be nearly 1.5 mmol/g [22,23]. The obtained results of the present investigation show that RB has a low CV^+ adsorption capacity (0.51 mmol/g) in comparison with SWy-1. This preference of adsorption exhibited by SWy-1 is due mainly to the its higher CEC (0.76 mmol/g).

The adsorption equilibrium data was also applied to the Freundlich model (Eq. (3)) [24] given below:

$$\log q_e = \log K_F + \frac{1}{n} \log C_e \quad (3)$$

where K_F and n are Freundlich constants related to adsorption capacity and adsorption intensity, respectively.

The Freundlich model constants and R^2 values presented in Table 3 prove that this model successfully fitted the experimental data when compared to the Langmuir model. The Freundlich adsorption capacity (K_F) was found to be 0.35 and 0.21 for the RB and 0.2-AAB samples, respectively. In the adsorption systems, n values are 1.30 and 3.63 which indicate that adsorption intensity is favorable over the entire range of concentrations studied.

3.4. Effects of temperature

The thermodynamic parameters were determined using the following equations:

$$\ln K_L = \frac{\Delta S}{R} - \frac{\Delta H}{RT} \quad (4)$$

$$\Delta G = \Delta H - T\Delta S \quad (5)$$

where K_L (L/mmol) is the Langmuir constant, ΔS, ΔH and ΔG are the changes of entropy, enthalpy and the Gibbs energy, T (K) is the temperature, R (J mol^{-1} K^{-1}) is the gas constant. The values of ΔH and ΔS were determined from the slopes and intercepts of the plots of ln K_L vs. $1/T$ (not shown).

As given in Table 4, the adsorption of the CV^+ onto bentonite samples is an endothermic process, which indicates that the amount of the adsorbed dye increases at higher temperatures. This may be attributed to the increased penetration of the CV^+ inside pores at higher temperatures or the generation of new adsorption sites. It is known that a large proportion of the active sites of the bentonite would be occupied by water molecules via hydrogen bonds. Furthermore, the molecular size of CV^+ is larger than that of water; therefore, one CV^+ cation adsorbed on active sites would replace

Table 3
Langmuir and Freundlich parameters for the adsorption of CV^+ onto bentonite samples.

Sample	Langmuir			Freundlich		
	q_m (mmol/g)	K_L (L/mmol)	R^2	n	K_F (mmol$^{(1-1/n)}$ L$^{1/n}$/g)	R^2
RB	0.51	0.95	0.983	1.30	0.35	0.993
0.2-AAB	0.23	1.60	0.982	3.63	0.21	0.998

Table 4
Thermodynamic parameters for the adsorption of CV^+ onto bentonite samples.

Sample	ΔH (kJ/mol)	ΔS (J/mol K)	ΔG (kJ/mol)				R^2
			290.15	308.15	318.15	338.15	
RB	62.1	245	−8.9	−13.4	−15.8	−20.7	0.976
0.2-AAB	45.5	193	−10.5	−13.9	−15.9	−19.8	0.918

more than one surface water molecule. CV^+ cations adsorbed on the surface released energy that was not strong enough to overcome the strong hydrogen bonding between the water molecules and the bentonite. Therefore, the overall adsorption reaction would absorb energy from the surrounding solution, which yields an endothermic reaction. Besides pore structure characteristics, the surface chemical characteristics are also important factors affecting the large organic cation adsorption behavior. These results also showed that the large organic cation adsorption process onto bentonites is accompanied not only by the ion-exchange but also the release of the water molecules. It is clear that the entropy of adsorption as follows: RB > 0.2-AAB. This means that the adsorption of CV^+ onto RB sample gives a less-ordered system than does the adsorption of CV^+ onto the 0.2-AAB sample. The positive values of ΔS suggest increased randomness at the solid/solution interface and significant changes occur on the surface of the bentonite through the CV^+ adsorption. The positive values of ΔS also suggest the randomness at the solid-solution interface increases during the adsorption process, since the CV^+ species adsorbed leads to a decrease in the number of the water molecules. The CV^+ cations are transported from the water constraint to the bentonite surface spontaneously to gain entropy. Furthermore, values of $T_{av}\Delta S$ can be calculated from the experimental data where T_{av} represents the average values of the range of temperature used for adsorption studies. It is found that $\Delta H < T_{av}\Delta S$ for the both type of bentonites. This means, although contribution of ΔH are not negligible, but the influence of entropies are more remarkable. The negative ΔG values indicate that the adsorption process is thermodynamically feasible at room temperature (Table 4). The different values of the thermodynamic parameters found for the RB and 0.2-AAB samples implicate a non-uniform thermodynamic process during the bentonite-CV^+ interaction.

3.5. Adsorption dynamics

It is also noticed in Figs. 3 and 4 that for $C_0 = 1.2$ mmol/g at 295.15 K, the equilibrium time was achieved after 250 min for RB and 130 min 0.2-AAB sample, respectively. The adsorption rate was fast and more than half of the adsorbed-CV^+ was removed in the first 55 min for RB and 25 min for 0.2-AAB at the room temperature. These results showed that in the initial stage of adsorption, a large number of vacant surface sites are available for adsorption. After the initial stage of adsorption, the remaining vacant surface sites are difficult to occupy due to repulsive forces between the CV^+ molecules on the bentonite surface and the bulk phase. This is due to the high concentration gradient in the beginning of adsorption which represents a high driving force for the transfer of CV^+ from solution to the surface of bentonites.

Several kinetic models are available to understand the behavior of the adsorbent and also to examine the controlling mechanism

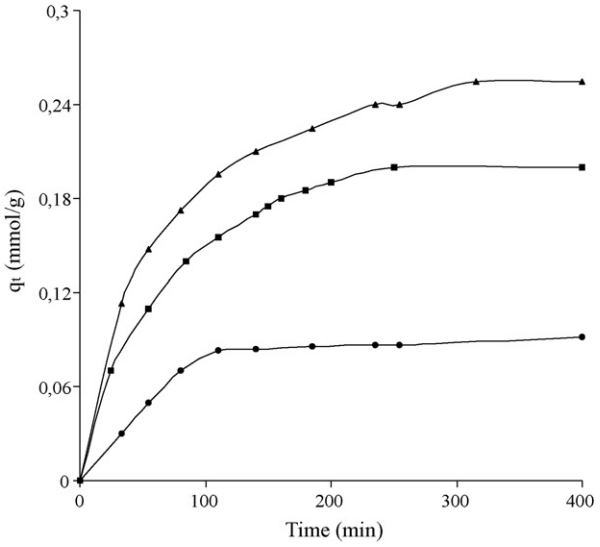

Fig. 3. Plots of adsorbed CV^+ amount vs. time onto the RB sample at different initial CV^+ concentrations. 0.1 mmol/g; circles, 0.6 mmol/g; squares, 1.2 mmol/g; triangles. $T = 295.15$ K, initial pH = 6.0, $m = 2$ g/L.

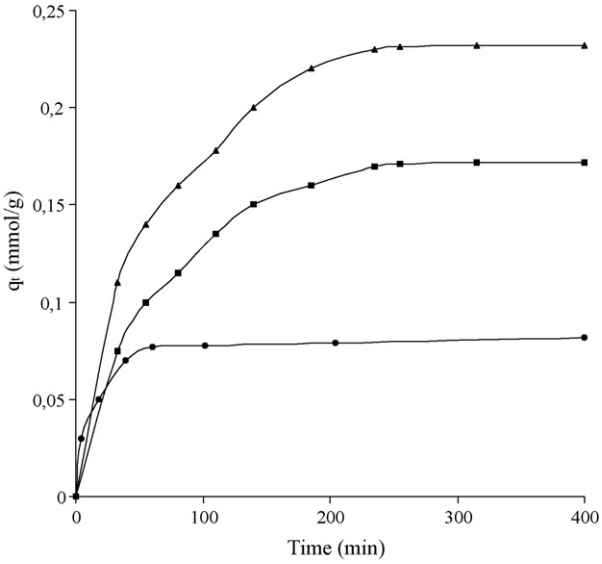

Fig. 4. Plots of adsorbed CV^+ amount vs. time onto the AAB sample at different initial CV^+ concentrations. 0.1 mmol/g; circles, 0.6 mmol/g; squares, 1.2 mmol/g; triangles. $T = 295.15$ K, initial pH = 6.0, $m = 2$ g/L.

Table 5
Kinetic parameters for the adsorption of CV^+ onto RB sample at different initial dye concentrations.

C_o (mmol/g)	$q_{e,cal}$ (mmol/g)	Pseudo-first order model			Pseudo-second order model		
		${R_1}^2$	$k_1 \times 10^2$ (1/min)	${R_2}^2$	$q_{e,2}$ (mmol/g)	$h \times 10^2$ (mmol/g min)	$k_2 \times 10^2$ (g/mmol min)
0.1	0.16	0.992	1.21	0.997	0.23	0.42	13.52
0.6	0.17	0.997	1.16	0.999	0.25	0.36	5.59
1.2	0.23	0.970	1.09	0.999	0.29	0.52	5.53

Table 6
Kinetic parameters for the adsorption of CV^+ onto AAB sample at different initial dye concentrations.

C_o (mmol/g)	$q_{e,cal}$ (mmol/g)	Pseudo-first order model			Pseudo-second order model		
		${R_1}^2$	$k_1 \times 10^2$ (1/min)	${R_2}^2$	$q_{e,2}$ (mmol/g)	$h \times 10^2$ (mmol/g min)	$k_2 \times 10^2$ (g/mmol min)
0.1	0.15	0.999	0.54	0.999	0.20	0.29	52.70
0.6	0.17	0.930	0.63	0.998	0.21	0.36	8.13
1.2	0.23	0.980	1.81	0.997	0.27	0.52	6.69

Table 7
Effect of surface area on pseudo-second order rate constant for the adsorption of CV^+ onto bentonite samples.

Sample	Surface area (m^2/g)	Micropore volume (cm^3/g)	q_m (mmol/g)	Pseudo-second order model	
				R^2	k_2 (g/mmol min)
RB	36	0.08	0.51	0.993	0.13
0.2-AAB	110	0.11	0.23	0.999	0.52
0.5-AAB	175	0.20	0.21	0.999	0.34
1.0-AAB	285	0.42	0.20	0.998	0.19
2.0-AAB	190	0.21	0.18	0.994	0.14

of the adsorption process and to test the experimental data. In the present investigation, the adsorption data were analyzed using two kinetic models, the pseudo-first order, and pseudo-second order kinetic models.

The pseudo-first order model was presented by Lagergren [25]. The Lagergren's first-order reaction model is expressed as follows:

$$\log(q_e - q_t) = \log\ q_e - \frac{k_1}{2.303}t \quad (6)$$

where q_e and q_t are the amounts of dye (mmol/g) adsorbed on the clay at equilibrium, and at time t, respectively and k_1 is the rate constant (min^{-1}). The rate constant, k_1 was obtained from slope of the linear plots of $\log(q_e - q_t)$ against t.

The adsorption data was also analyzed in terms of pseudo-second-order mechanism, described by Ho and McKay [26].

$$\frac{t}{q_t} = \frac{1}{h} + \frac{1}{q_e}t \quad (7)$$

and the initial rate of adsorption h is:

$$h = k_2 {q_e}^2 \quad (8)$$

where k_2 is the rate constant of pseudo-second order adsorption (g/mmol min), h is the initial rate of adsorption (mmol/g min). If second-order kinetics is applicable, the plot of t/q_t against t of Eq. (7) should give a linear relationship from which the constants q_e, h and k_2 can be determined.

Tables 5 and 6 list the results of the rate constant studies for different initial dye concentrations by the pseudo-first order and pseudo-second order models at 295.15 K. It is seen that the correlation coefficient of pseudo-first order kinetic are lower than in the case of pseudo-second order kinetic model. This finding shows that kinetics of dye adsorption by bentonites are better described by pseudo-second order kinetic model rather than pseudo-first order model. As given in Tables 5 and 6, the rate constant of CV^+ uptake was found to decrease from 13.52×10^{-2} to 5.53×10^{-2} g/mmol min for RB and the rate constants for the 0.2-AAB decreased with the increase of the initial dye concentration (from 52.70×10^{-2} to 6.69×10^{-2} mmol/g min).

The effect of adsorbent surface area on CV^+ uptakes for five different bentonite sample is given in Table 7. It is obvious that for higher surface area, which have a higher solid–liquid interfacial area, the adsorption rates is higher. A linear relationship exists between the adsorption rate and the surface area, as evidenced by the R^2 values being close to unity (36 m^2/g, $R^2 = 0.993$; 95 m^2/g, $R^2 = 0.999$; 175 m^2/g, $R^2 = 0.999$; 285 m^2/g, $R^2 = 0.999$ and 190 m^2/g, $R^2 = 0.994$). Such an effect is probably due to the ability of the large dye molecule to penetrate the pore structure of the bentonite. It can be concluded that the adsorption rates of CV^+ over four acid activated bentonite samples are higher than that over RB, which may be resulted from the higher surface area of AAB than RB. CV^+ molecules can easily diffuse into the pores of AABs. On the other hand, RB had the lowest accessible surface area among all bentonites but it showed higher uptake than the best performing activated bentonite. The higher uptake of RB was attributed to its more basic surface.

These results indicate the possibility of AAB using in separation of large organic cation from water. For example, the q_m value for RB was about 1.24 times larger than that for 0.2-AAB but the k_2 value was 3.90 times smaller, under comparable conditions ($C_0 = 0.1$ mmol/g). The application potential of acid activated bentonites for adsorption removal of large organic cation from aqueous streams can be highlighted.

4. Conclusions

It was concluded from the equilibrium and kinetic data that the amount of CV^+ adsorbed over RB was higher than that of AAB. The Freundlich model agrees with experimental data well. It was found that the kinetics of the adsorption of CV^+ onto bentonite samples at different initial concentrations was the best described by the pseudo-second order model. The rate parameters of the intra-particle diffusion model for adsorption were also evaluated and compared the adsorption mechanisms. Also, the analysis of these thermodynamic parameters showed that the CV^+ adsorption onto both type of bentonites is mainly physical process.

References

[1] E.N. El Qada, S.J. Allen, G.M. Walker, Adsorption of basic dyes from aqueous solution onto activated carbons, Chem. Eng. J. 135 (2008) 174–184.
[2] S.S. Tahir, R. Naseem, Removal of Cr(III) from tannery wastewater by adsorption onto bentonite clay, Sep. Purif. Technol. 53 (2007) 312–321.
[3] E. Eren, B. Afsin, An investigation of Cu(II) adsorption by raw and acid-activated bentonite: a combined potentiometric, thermodynamic, XRD, IR, DTA study, J. Hazard. Mater. 151 (2008) 682–691.
[4] Z. Rawajfih, N. Nsour, Characteristics of phenol and chlorinated phenols sorption onto surfactant-modified bentonite, J. Colloid Interface Sci. 298 (2006) 39–49.
[5] S. Andini, R. Cioffi, F. Montagnaro, F. Pisciotta, L. Santoro, Simultaneous adsorption of chlorophenol and heavy metal ions on organophilic bentonite, Appl. Clay Sci. 31 (2006) 126–133.
[6] A. Demirbas, A. Sari, O. Isildak, Adsorption thermodynamics of stearic acid onto bentonite, J. Hazard. Mater. 135 (2006) 226–231.
[7] F. Ayari, E. Srasra, M. Trabelsi-Ayadi, Retention of organic molecule "quinalizarin" by bentonitic clay saturated with different cations, Desalination 206 (2007) 499–506.
[8] T. Asselman, G. Garnier, Adsorption of model wood polymers and colloids on bentonites, Colloids Surf. A 168 (2000) 175–182.
[9] M.M. Bacquet, B. Morcellet, M. Benabadji, K.I. Medjahed, K. Mansri, A. Meniai, A.-H. Bencheikh Lehocine, Adsorption of poly(4-vinylpyridine) onto bentonites, Mater. Lett. 58 (2004) 455–459.
[10] E. Bojemueller, A. Nennemann, G. Lagaly, Enhanced pesticide adsorption by thermally modified bentonites, Appl. Clay Sci. 18 (2001) 277–284.
[11] J. Bors, S. Dultz, B. Riebe, Organophilic bentonites as adsorbents for radionuclides: I. Adsorption of ionic fission products, Appl. Clay Sci. 16 (2000) 1–13.
[12] Q.-Y. Yue, Q. Li, B.-Y. Gao, Y. Wang, Kinetics of adsorption of disperse dyes by polyepicholorohydrin-dimethylamine cationic polymer/bentonite, Sep. Purif. Technol. 54 (2007) 279–290.
[13] E. Eren, B. Afsin, Investigation of a basic dye adsorption from aqueous solution onto raw and pre-treated bentonite surfaces, Dyes Pigments 76 (2008) 220–225.
[14] R. Dohrmann, Cation exchange capacity methodology. I: an efficient model for the detection of incorrect cation exchange capacity and exchangeable cation results, Appl. Clay Sci. 34 (2006) 31–37.
[15] E. Eren, J. Hazard. Mater., doi:10.1016/j.jhazmat.2008.06.016.
[16] M. Onal, Y. Sarıkaya, Preparation and characterization of acid-activated bentonite powders, Powder Technol. 172 (2007) 14–18.
[17] K.G. Bhattacharyya, S.S. Gupta, Adsorption of Fe(III) from water by natural and acid activated clays: studies on equilibrium isotherm, kinetics and thermodynamics of interactions, Adsorption 12 (2006) 185–204.
[18] G.J. Churchman, W.P. Gates, B.K.G. Theng, G. Yuan, Clays and clay minerals for pollution control, in: F. Bergaya, B.K.G. Theng, G. Lagaly (Eds.), Handbook of Clay Science, Elsevier, Amsterdam, 2006, pp. 625–675.
[19] G. Lagaly, M. Ogawa, I. Dékány, Clay mineral–organic interactions, in: F. Bergaya, B.K.G. Theng, G. Lagaly (Eds.), Handbook of Clay Science, Elsevier, Amsterdam, 2006, pp. 309–377.
[20] C.B. Hedley, G. Yuan, B.K.G. Theng, Thermal analysis of montmorillonites modified with quaternary phosphonium and ammonium surfactants, Appl. Clay Sci. 35 (2007) 180–188.
[21] I. Langmuir, The adsorption of gases on plane surfaces of glass, mica and platinum, J. Am. Soc. 40 (1918) 1361–1403.
[22] G. Rytwo, C. Serban, S. Nir, L. Margulies, Use of methylene blue and crystal violet for determination of exchangeable cations in montmorillonite, Clays Clay Miner. 39 (1991) 551–555.
[23] S. Nir, G. Rytwo, U. Yermiyahu, L. Margulies, A model for cation adsorption to clays and membranes, Colloid Polym. Sci. 272 (1994) 619–632.
[24] H. Freundlich, Über die adsorption in lösungen, Zeitschrift für Physikalische Chemie 57 (1906) 385–470.
[25] S. Lagergren, Zur theorie der sogenannten adsorption gelöster stoffe. Kungliga Svenska Vetenskapsakademiens, Handlingar, 24 (1898) 1–39.
[26] Y.S. Ho, G. McKay, Comparative sorption kinetic studies of dye and aromatic compounds onto fly ash, J. Environ. Sci. Health A 34 (1999) 1179–1204.